

Prospects of medium tomography using back-to-back hadron correlations

Thorsten Renk* and Kari J. Eskola†

*Department of Physics, P.O. Box 35 FI-40014 University of Jyväskylä, Finland and
Helsinki Institute of Physics, P.O. Box 64 FI-00014, University of Helsinki, Finland*

We discuss the prospects of extracting information about the bulk QCD matter distribution and evolution on the basis of hard hadronic back-to-back correlations in ultrarelativistic heavy-ion collisions. Using both hydrodynamical and parametrized evolution models for the spacetime evolution of the produced matter, which have been tested against RHIC data, we study six different setups for the spacetime dependence of hard-parton energy losses. Assuming that the energy loss of hard partons traversing the medium is radiative and calculable in the BDMPS formalism, we adjust one parameter, the quenching power scale, to the measured R_{AA} in each of the setups and study the systematic variations of the back-to-back yield as a function of p_T . We show which spacetime regions are probed by one-particle and two-particle observables and study the role of longitudinal and transverse expansion in some detail. We also comment on the importance of considering fluctuations around the average energy loss. We conclude that while current data are too limited in momentum coverage, future data for higher trigger energy might provide the lever arm in away side hadron momentum necessary to perform medium tomography, provided that sufficient precision can be achieved.

PACS numbers: 25.75.-q, 25.75.Gz

I. INTRODUCTION

Announcements have been made by all four detector collaborations at RHIC [1] that a new state of matter, distinct from ordinary hadronic matter, has been created in ultrarelativistic heavy-ion collisions (URHIC). A new and exciting challenge for both experiment and theory is now to study its properties. The energy loss of hard partons created in the first moments of the collision has long been regarded a promising tool for this purpose [2, 3, 4, 5, 6, 7].

So far, most of the effort in parton energy loss studies has been directed to understanding the nuclear suppression factor R_{AA} , i.e. the observed transverse momentum spectrum of hard hadrons divided by the scaled expectation from proton-proton collisions. However, as recently argued in [8], R_{AA} exhibits only very limited sensitivity to the energy loss mechanism or properties of the medium beyond the fact that the quenching of jets is substantial. Thus, in order to overcome this obstacle and gain information about the medium properties, one possibility outlined in [8] is to measure the momentum spectrum of hadrons correlated with a hard real photon at fixed energy. This has been shown to be able to discriminate between different scenarios of energy loss.

In principle more detailed information about the energy loss mechanism and the medium is also available in back-to-back hadron correlations. Measurements of two-particle correlations involving one hard trigger particle and associate hadrons above 1 GeV have shown a surprising splitting of the away side peak for all centralities but peripheral collisions, qualitatively very different from

a broadened away side peak observed in p-p or d-Au collisions [9]. Interpretations in terms of energy lost to propagating colourless [10, 11, 12] and coloured [13] sound modes have been suggested for this phenomenon, and calculations within a dynamical model evolution have shown that the data can be reproduced under the assumption that a substantial amount of lost energy excites a sonic shockwave [10]. Thus, it appears that for semi-hard associate hadron momentum scales the recoil of the soft bulk medium is probed rather than the energy loss of the hard parton. While properties of the medium can be inferred from these measurements as well [14], this is outside the scope of the present paper where we focus on the measurement of energy loss in hard back-to-back correlations.

For sufficiently high associate hadron transverse momentum $P_T > 4$ GeV, back-to-back correlations with vacuum width are observed experimentally [15, 16] and the measured yield per trigger is in agreement with the expectation from radiative energy loss in a dynamic medium [17]. As argued in [8], a measurement of R_{AA} , or more general the suppression of a single hadron observable probes an averaged energy loss probability distribution $\langle P(\Delta E, E) \rangle_{T_{AB}}$ where the averaging is done over all possible initial vertex positions (determined by the nuclear overlap T_{AB}) and the soft matter. However, in two particle correlations, the requirement that a trigger hadron is observed leads to a geometrical bias, and thus the yield per trigger of away side hadrons is determined by a different averaged energy loss probability $\langle P(\Delta E, E) \rangle_{Tr}$ where the averaging is done over all vertices leading to a triggered event. Thus, e.g. the distribution of away side pathlengths will be very different from the distribution underlying R_{AA} . The question we would hence like to address is whether the difference between $\langle P(\Delta E, E) \rangle_{T_{AB}}$ and $\langle P(\Delta E, E) \rangle_{Tr}$ is (dependent on the medium evolu-

*Electronic address: trenk@phys.jyu.fi

†Electronic address: kari.eskola@phys.jyu.fi

tion model) significant enough to infer non-trivial information about the medium, or in other words, to what extent there is information in back-to-back correlations beyond the information carried by R_{AA} .

Our strategy to investigate the question is as follows:

1. We consider two types of models for the medium evolution which reproduce the observed bulk characteristics of Au-Au collisions at full RHIC energy $\sqrt{s_{NN}} = 200$ GeV.

Type I is the longitudinally boost-invariant hydrodynamical evolution model discussed in [18], where the multiplicities and transverse momentum spectra of pions, kaons and protons in Au-Au collisions at $\sqrt{s_{NN}} = 130$ GeV are used as constraints and the initial conditions are computed from perturbative QCD+saturation [19]. Type II is the parametrized evolution model of Ref. [20], where in addition to the P_T spectra also the rapidity distribution [21] and Hanbury-Brown-Twiss (HBT) correlations [22] of central 200 AGeV Au-Au collisions at RHIC are required to be reproduced.

2. The energy losses of hard partons in the evolving medium we then describe by the BDMPS mechanism in the form presented in Ref. [23]. Assuming that partons lose energy either during the entire evolution or in the QGP phase only (in the hydrodynamic model), and varying the initial matter density profiles in the Type 2 parametrized model, we discuss six different cases for the spacetime dependence of the hard parton energy losses. In each case, we adjust one parameter, the scale of the quenching power, so that the measured R_{AA} is reproduced. We discuss how R_{AA} arises from $\langle P(\Delta E, E) \rangle_{T_{AB}}$ and which geometrical regions are probed for each case. In particular, we comment on the role of surface bias.

3. Keeping all model parameters fixed from this point, we proceed to calculate the yield per trigger for back-to-back correlations for each of the 6 cases. For this purpose, we use a Monte Carlo simulation of the trigger setting as outlined in [17]. While each model leads (by construction) to almost identical R_{AA} , we find systematic differences in the back-to-back yields for different associate momentum bins. We discuss both a scenario with the present highest trigger $8 \text{ GeV} < p_T < 15 \text{ GeV}$ and the prospects for a higher trigger $15 \text{ GeV} < p_T < 20 \text{ GeV}$. In order to understand what spacetime region of the evolution is probed in these simulations, we discuss the distributions of vertices in triggered events and dihadron events for each scenario in detail. We compare with current data from STAR [15, 16] and comment on the prospects of probing medium properties in back-to-back correlation measurements as well as uncertainties in the results.

II. THE FRAMEWORK

Our framework setup consists of three main parts: The hard process which is calculated in perturbative QCD

(pQCD), supplemented by fragmentation of a hard parton outside the medium, the bulk matter evolution for which we either use a hydrodynamic [18] (Type 1; 2 cases) or a parametrized evolution model [20] (Type 2; 4 cases) and the energy loss probability distribution given a hard parton path through the soft medium [23]. In the following we describe the implementation of each of these ingredients in turn.

A. The unmodified hard process

In Ref. [24] it has been demonstrated that leading order (LO) pQCD is rather successful in describing the p_T -spectrum of inclusive hadron production over a wide range in \sqrt{s} when supplemented by a \sqrt{s} -dependent K -factor to adjust the overall normalization. This factor parametrizes next-to-leading order effects. Since we are in the following only interested in ratios of P_T -distributions, i.e. observed yield of hadrons in A-A collision divided by scaled yield in p-p collision, or yields per trigger, any factor independent of p_T drops out. Hence, in the following we use LO pQCD expressions without trying to adjust absolute normalization.

The production of two hard partons k, l in LO pQCD is described by

$$\frac{d\sigma^{AB \rightarrow kl+X}}{dp_T^2 dy_1 dy_2} = \sum_{ij} x_1 f_{i/A}(x_1, Q^2) x_2 f_{j/B}(x_2, Q^2) \frac{d\hat{\sigma}^{ij \rightarrow kl}}{d\hat{t}} \quad (1)$$

where A and B stand for the colliding objects (protons or nuclei) and $y_{1(2)}$ is the rapidity of parton $k(l)$. The distribution function of a parton type i in A at a momentum fraction x_1 and a factorization scale $Q \sim p_T$ is $f_{i/A}(x_1, Q^2)$. The distribution functions are different for the free protons [25, 26] and protons in nuclei [27, 28]. The fractional momenta of the colliding partons i, j are given by $x_{1,2} = \frac{p_T}{\sqrt{s}} (\exp[\pm y_1] + \exp[\pm y_2])$.

Expressions for the pQCD subprocesses $\frac{d\hat{\sigma}^{ij \rightarrow kl}}{d\hat{t}}(\hat{s}, \hat{t}, \hat{u})$ as a function of the parton Mandelstam variables \hat{s}, \hat{t} and \hat{u} can be found e.g. in [29]. Inclusive production of a parton flavour f at rapidity y_f is found by integrating over either y_1 or y_2 and summing over appropriate combinations of partons,

$$\begin{aligned}
\frac{d\sigma^{AB \rightarrow f+X}}{dp_T^2 dy_f} = \int dy_2 \sum_{\langle ij \rangle, \langle kl \rangle} \frac{1}{1 + \delta_{kl}} \frac{1}{1 + \delta_{ij}} \left\{ x_1 f_{i/A}(x_1, Q^2) f_{j/B}(x_2, Q^2) \left[\frac{d\sigma^{ij \rightarrow kl}}{d\hat{t}}(\hat{s}, \hat{t}, \hat{u}) \delta_{fk} + \frac{d\sigma^{ij \rightarrow kl}}{d\hat{t}}(\hat{s}, \hat{u}, \hat{t}) \delta_{fl} \right] \right. \\
\left. + x_1 f_{j/A}(x_1, Q^2) f_{i/B}(x_2, Q^2) \left[\frac{d\sigma^{ij \rightarrow kl}}{d\hat{t}}(\hat{s}, \hat{u}, \hat{t}) \delta_{fk} + \frac{d\sigma^{ij \rightarrow kl}}{d\hat{t}}(\hat{s}, \hat{t}, \hat{u}) \delta_{fl} \right] \right\}
\end{aligned} \quad (2)$$

where the summation $\langle ij \rangle, \langle kl \rangle$ runs over pairs $gg, gq, g\bar{q}, qq, q\bar{q}, \bar{q}\bar{q}$ and q stands for any of the quark flavours u, d, s .

For the production of a hadron h with mass M , transverse momentum P_T at rapidity y and transverse mass $m_T = \sqrt{M^2 + P_T^2}$ from the parton f , let us introduce the fraction z of the parton energy carried by the hadron after fragmentation with $z = E_h/E_f$. Assuming collinear fragmentation, the hadronic variables can be written in terms of the partonic ones as

$$m_T \cosh y = z p_T \cosh y_f \quad \text{and} \quad m_T \sinh y = P_T \sinh y_f. \quad (3)$$

Thus, the hadronic momentum spectrum arises from the partonic one by folding with the probability distribution $D_{f \rightarrow h}(z, \mu_f^2)$ to fragment with a fraction z at a scale $\mu_f \sim P_T$ as

$$\frac{d\sigma^{AB \rightarrow h+X}}{dP_T^2 dy} = \sum_f \int dp_T^2 dy_f \frac{d\sigma^{AB \rightarrow f+X}}{dp_T^2 dy_f} \int_{z_{min}}^1 dz D_{f \rightarrow h}(z, \mu_f^2) \delta(m_T^2 - M_T^2(p_T, y_f, z)) \delta(y - Y(p_T, y_f, z)) \quad (4)$$

with

$$M_T^2(p_T, y_f, z) = (z p_T)^2 + m^2 \tanh^2 y_f \quad (5)$$

and

$$Y(p_T, y_f, z) = \text{arsinh} \left(\frac{P_T}{m_T} \sinh y_f \right) \quad (6)$$

where m is the parton mass. The lower cutoff $z_{min} = \frac{2m_T}{\sqrt{s}} \cosh y$ arises from the fact that there is a kinematical limit on the parton momentum; it cannot exceed $\sqrt{s}/(2 \cosh y_f)$ and thus for given hadron momentum there is a minimal z corresponding to fragmentation of a parton with maximal momentum. In the following, we use the KKP set of fragmentation functions $D_{f \rightarrow h}(z, \mu_f^2)$ [30].

B. Energy loss of a hard parton in the soft medium

The key quantity characterizing the energy loss induced by a medium with energy density ϵ in the BDMPS formalism is the local transport coefficient $\hat{q}(\tau, \eta_s, r)$ which characterizes the squared average momentum transfer from the medium to the hard parton per unit pathlength. Since we consider a time-dependent inhomogeneous medium, this quantity depends on proper time

$\tau = \sqrt{t^2 - z^2}$, spacetime rapidity $\eta_s = \frac{1}{2} \ln \frac{t+z}{t-z}$, cylindrical radius r and in principle also on azimuthal angle ϕ , but for the time being we focus on central collisions only.

The transport coefficient is related to the energy density of the medium as

$$\hat{q}(\tau, \eta_s, r) = K \cdot 2 \cdot [\epsilon(\tau, \eta_s, r)]^{3/4} \quad (7)$$

with $K = 1$ for an ideal quark-gluon plasma (QGP) [31]. In the following, motivated by Ref. [31] we assume the proportionality constant K to remain unaltered in different phases of the medium. We treat K as an adjustable parameter for the following reasons: First, the energy loss of a parton propagating through the medium scales with the strong coupling α_s . While we assume $\alpha_s = 0.45$ throughout the energy loss calculation (and thus scale the \hat{q} of Ref. [23] accordingly with 0.45/0.33), the precise value of the parameter is not known and may be substantially larger [32]. Second, we calculate energy loss only from the onset of thermalization but there will in all likelihood be some contribution from processes before thermalization which in principle should be accounted for. Third, there may also be a contribution from elastic energy loss [33], which we do not include here, either. While the hard dihadron correlation pattern suggests that this is not dominant [17] it may still contribute.

Fourth, the temperature range probed at RHIC seems to be relatively close ($T \leq 3T_C$) to the phase transition, thus calculating the transport coefficient in a perturbative expansion may be conceptually problematic (see [34] for a non-perturbative definition of \hat{q} and an evaluation in the strong coupling limit using AdS/CFT).

Given the local transport coefficient at each spacetime point, a parton's energy loss depends on the position of the hard vertex at $\mathbf{r}_0 = (x_0, y_0)$ in the transverse plane at $\tau = 0$ and the angular orientation of its trajectory ϕ (i.e. its path through the medium). To the degree to which the medium changes as a function of y , there is also a weak dependence on rapidity (in models of Type 2 considered here). In order to determine the probability $P(\Delta E, E)_{path}$ for a hard parton with energy E to lose the energy ΔE while traversing the medium on its trajectory, we make use of a scaling law [35] which allows to relate the dynamical scenario to a static equivalent one by calculating the following quantities averaged over the jet trajectory $\xi(\tau)$:

$$\omega_c(\mathbf{r}_0, \phi) = \int_0^\infty d\xi \xi \hat{q}(\xi) \quad (8)$$

and

$$\langle \hat{q}L \rangle(\mathbf{r}_0, \phi) = \int_0^\infty d\xi \hat{q}(\xi) \quad (9)$$

as a function of the jet production vertex \mathbf{r}_0 and its angular orientation ϕ . We set $\hat{q} \equiv 0$ whenever the decoupling temperature of the medium $T = T_F$ is reached. In the presence of flow, we follow the prescription outlined in [36, 37] and replace

$$\hat{q} = K \cdot 2 \cdot \epsilon^{3/4}(p) \rightarrow K \cdot 2 \cdot \epsilon^{3/4}(T^{n \perp n \perp}) \quad (10)$$

with

$$T^{n \perp n \perp} = p(\epsilon) + [\epsilon + p(\epsilon)] \frac{\beta_\perp^2}{1 - \beta_\perp^2} \quad (11)$$

where β_\perp is the spatial component of the flow field orthogonal to the parton trajectory. In the above two expressions, the spacetime dependence (η_s, r, τ) of pressure p and energy-momentum tensor $T^{n \perp n \perp}$ have been suppressed for clarity.

Using the numerical results of [23], we obtain $P(\Delta E)_{path}$ for ω_c and $R = 2\omega_c^2/\langle \hat{q}L \rangle$ [38] as a function of jet production vertex and the angle ϕ corresponding to

$$P(\Delta E)_{path} = \sum_{n=0}^{\infty} \frac{1}{n!} \left[\prod_{i=1}^n \int d\omega_i \frac{dI(\omega_i)}{d\omega} \right] \delta \left(\Delta E - \sum_{i=1}^n \omega_i \right) \exp \left[- \int d\omega \frac{dI}{d\omega} \right] \quad (12)$$

which makes use of the distribution $\omega \frac{dI}{d\omega}$ of gluons emitted into the jet cone. The explicit expression of this quantity for the case of multiple soft scattering can be found in [23]. Note that the formalism of [23] is defined for the limit of asymptotic parton energy, hence the probability distribution obtained $P(\Delta E)_{path}$ is independent of E .

The initially produced hard parton spectrum and, consequently, the number of hard vertices in the (x, y) plane (where the z -axis is given by the beam direction) in an $A - A$ collision at fixed impact parameter \mathbf{b} , are proportional to the nuclear overlap,

$$\frac{dN_{AA}^f}{dq_T^2 dy_f^*} = T_{AA}(0) \frac{d\sigma^{AA \rightarrow f+X}}{dq_T^2 dy_f^*}, \quad (13)$$

where $T_{AA}(\mathbf{b})$ is the standard nuclear overlap function and the cross section is from Eq. (2). The asterisks denote the jet state before any energy losses. We define a

normalized geometrical distribution $P(x_0, y_0)$ for central collisions as

$$P(x_0, y_0) = \frac{[T_A(\mathbf{r}_0)]^2}{T_{AA}(0)}, \quad (14)$$

where the thickness function is given in terms of Woods-Saxon the nuclear density $\rho_A(\mathbf{r}, z)$ as $T_A(\mathbf{r}) = \int dz \rho_A(\mathbf{r}, z)$.

Thus, we can define the averaged energy loss probability distribution [8] as

$$\langle P(\Delta E) \rangle_{T_{AA}} = \frac{1}{2\pi} \int_0^{2\pi} d\phi \int_{-\infty}^{\infty} dx_0 \int_{-\infty}^{\infty} dy_0 P(x_0, y_0) P(\Delta E)_{path}. \quad (15)$$

In the following, we assume that energy loss and fragmentation are cleanly separable, i.e. energy loss happens on the partonic level, then the hard parton emerges from

the medium and undergoes fragmentation in vacuum. In practice this seems to be realized for hadrons with $p_T > 6$ GeV (cf. [17]). Assuming that this condition is fulfilled, and that the direction ϕ of an outgoing parton is not significantly changed, and only its energy E_i is reduced by ΔE , we define an effective in-medium analogue for Eq. (2), i.e. spectrum of partons which have experienced energy losses (not a true cross section as it is computed

at a fixed impact parameter),

$$\frac{d\tilde{\sigma}_{medium}^{AA \rightarrow f+X}}{dp_T dy_f} \equiv \frac{1}{T_{AA}(0)} \frac{dN_{AA}^f}{dp_T dy_f}. \quad (16)$$

By folding in Eqs. (13) and (15), we obtain

$$\frac{d\tilde{\sigma}_{medium}^{AA \rightarrow f+X}}{dp_T dy_f} = \int d\Delta E \langle P(\Delta E) \rangle_{T_{AA}} \int dq_T dy_f^* d\phi_f^* \frac{d\sigma^{AB \rightarrow f+X}}{dq_T dy_f^*} \delta(y_f - y_f^*) \delta(p_T - (q_T - \Delta E)) \delta(\phi - \phi_f^*), \quad (17)$$

where again q_T , y_f^* and ϕ_f^* are parton's kinematic quantities before the energy loss. Inserting Eq. (17) into Eq. (4) yields the medium-modified spectrum

$$\frac{d\tilde{\sigma}_{medium}^{AA \rightarrow h+X}}{dP_T^2 dy} \equiv \frac{1}{T_{AA}(0)} \frac{dN_{AA}^h}{dP_T^2 dy} \quad (18)$$

of hadrons originating from hard processes.

The nuclear modification factor for central collision is defined as

$$R_{AA}(p_T, y) = \frac{dN_{AA}^h/dP_T dy}{T_{AA}(0) d\sigma^{pp}/dP_T dy}. \quad (19)$$

With the definitions above, we now obtain it as the ratio

$$R_{AA}(p_T, y) = \frac{d\tilde{\sigma}_{medium}^{AA \rightarrow h+X}}{dP_T^2 dy} / \frac{d\sigma^{pp \rightarrow h+X}}{dP_T^2 dy} \quad (20)$$

as we have taken into account the proper geometry and scaling already in the definition of $\langle P(\Delta E) \rangle_{T_{AA}}$.

C. Monte Carlo sampling of hard dihadron correlations

While we are able to solve Eqs. (4,15,17,20) using standard numerical multiple-dimensional integration routines in order to obtain R_{AA} from the model, due to the greater complexity of the problem we have to rely on Monte Carlo (MC) simulations to obtain the yield per trigger of dihadron correlations (note that this is different from [39] where Monte Carlo techniques are already used to obtain R_{AA}). For sufficient statistics, the techniques should not lead to different results and we have verified that R_{AA} can be computed also within the MC simulation with (within errors) identical results.

Let us briefly explain the procedure. First, we sample the distribution of partons emerging from a hard vertex determined by Eq. (1). This yields the parton type

(quark or gluon) as well as the transverse momentum. We define randomly one of the partons as 'near side' and propagate it to the surface of the medium. Along the path, we determine ω_c and $\langle \hat{q}L \rangle$ by evaluating Eqs. (8, 9). The resulting values serve as input for the probability distribution of energy loss $P(\Delta E)_{path}$ as determined in [23].

Often the plasma frequency ω_c is far above the available jet energy and $P(\Delta E)$ thus extends to energies $\Delta E \gg E_{jet}$. This reflects the fact that the radiative energy loss in [23] is derived in the limit of infinite parton energy. We consider a parton as absorbed by the thermal medium (and hence not tractable in the formalism outlined above) if its energy after energy loss is less than 0.5 GeV. Thus, in a significant number of cases the resulting outcome of energy loss will be absorption of the hard parton.

We determine the actual energy loss of the near side parton by sampling $P(\Delta E)_{path}$. To find the energy of the leading hadron, we need the probability $P_{f \rightarrow h}(z, \mu)$ to find a leading hadron with momentum fraction z at scale μ . Strictly speaking, this is not the fragmentation function as the fragmentation function yields the full single hadron distribution, not only the leading hadron, but since the trigger condition enforces on average large values of z , the two are virtually identical and we use the (normalized) fragmentation function $D_{f \rightarrow h}(z, \mu)$ as a model for $P_{f \rightarrow h}(z, \mu)$. Since the scale z_{min} (cf. Eq. (4)) cannot be implemented in the same way an approach starting from known parton properties before fragmentation (the hadronic m_T is not known at this point) we use a cutoff scale which is adjusted to RHIC d-Au data (see [17] for details). This introduces a (small) uncertainty in the absolute magnitude of the results once we scale the trigger energy upward from the measured data, as the cutoff scale should in principle also be altered. It does not alter the main result of the paper, i.e. the relative normalization of results for different models of medium evolution.

If the resulting hadronic $P_h = z p_f \approx z E_f$ fulfills the trigger condition we accept the event and proceed with the calculation of associated hadrons and the away side

parton, otherwise we reject the event and continue the MC sampling by generating a new vertex.

If an event fulfilling the trigger has been created, we determine the k_T smearing being added to the away side parton momentum. We sample a Gaussian distribution chosen such that the widening of the away side cone without a medium is reproduced. Since this is a number of order 1 GeV whereas partons fulfilling trigger conditions have frequently in excess of 15 GeV we note that this is a small correction.

We treat the far side parton exactly like the near side parton, i.e. we evaluate Eqs. (8, 9) along the path and find the actual energy loss from $P(\Delta E)$ with $\omega_c, \langle \hat{q}L \rangle$ as input. If the away side parton emerges with a finite energy, we again use the normalized fragmentation function $D_{f \rightarrow h}(z, \mu)$ to determine the momentum of the leading away side hadron. If this momentum fulfills the imposed P_T -trigger condition for associated particle production, we count the event as 'punchthrough'.

In addition, we allow for the possibility that the fragmentation of near and away side parton produces more than one hard hadron. We cannot simply subsume this in the fragmentation function as done for single hadron distributions as we are explicitly interested in the correlation strength between near side trigger hadron and other near side hadrons, thus we have to calculate sub-leading fragmentation processes separately. The quantity we need is $P_{f \rightarrow i}(z_1, z_2, \mu)$, i.e. the conditional probability to find a hadron i from a parent parton f with momentum fraction z_2 given that we already produced a leading hadron f with momentum fraction z_1 . In this language, the whole jet arises from a tower of conditional probabilities for higher order fragmentation processes. However, since we only probe the part of this tower resulting in hard hadrons, the treatment simplifies considerable.

Moreover, since we are predominantly interested in the quenching properties of the medium and not in detailed modelling of hadron distributions inside the jet, we model the next-to-leading conditional fragmentation probability using the measured probability distribution $A_i(z_F)$ of associated hadron production in d-Au collisions [15, 16] as a function of z_T where z_T is the fraction of the trigger hadron momentum carried by the associated hadron. We include a factor $\theta(E_i - E_{\text{trigger}} - \Delta E - E_{\text{assoc}})$ on the near side and $\theta(E_i - E_{\text{punch}} - \Delta E - E_{\text{assoc}})$ on the far side to make sure that energy is conserved. Note that associated production on the far side above the p_T cut is only possible if a punchthrough occurs. We count these events as 'near side associate production' and 'away side associated production'.

Thus, the yield per trigger for dihadron correlations on the near side is determined by the sum of all 'near side associate production' events divided by the number of events fulfilling the trigger, the yield per trigger on the away side is given by the sum of 'punchthrough' and 'away side associated production' divided by the number of events (fulfilling the near side trigger condition). These quantities can be directly compared to experiment.

D. Models for the medium evolution

The medium enters the formalism through Eq. (10) which specifies the transport coefficient as a function of local energy density ϵ and flow β_\perp and through the upper limit in the line integrals along the parton path Eqs. (8, 9) which are terminated once the decoupling condition of soft matter $T = T_F$ with T_F the decoupling temperature is reached.

As outlined in Sec. I, we consider two different types of models for the QCD matter spacetime evolution: hydrodynamics with pQCD+saturation initial conditions [18] and a parametrized evolution model [20]. Below, we briefly describe the main characteristics of these models, more details can be found in the original publications. Within these models, we study the six different setups for the energy losses shown in Fig. 1.

Type I: Hydrodynamic evolution

In the model [18] we use here, the hydrodynamical equations are solved in the transverse plane assuming a longitudinal Bjorken expansion and boost-invariance. The initial conditions, the initial energy densities, net-baryon number and formation time, are calculated from the pQCD + (final state) saturation model [19], where also next-to-leading order pQCD effects [41] are effectively taken into account. This approach correctly predicted the multiplicities in central Au+Au collisions at various cms-energies at RHIC. To describe the multiplicities and spectra of bulk hadrons, a decoupling temperature $T_F = 150$ MeV is needed [18, 40]. The initial energy density profile (which is correlated with the development of transverse flow and thus T_F) is assumed to be $\epsilon(\mathbf{r}_0) \propto [T_A(\mathbf{r}_0)]^2$. Thermalization is assumed to occur right at formation at $\tau_0 = 0.17$ fm/c for 5% central Au+Au collisions at $\sqrt{s_{NN}} = 200$ GeV. At this early time, a peak energy density of 220 GeV/fm³ is found in the center of the system, i.e. in a small volume. This value then decreases quickly as a function of time as the system expands. A bag equation of state is used and the system undergoes a 1st order phase transition from QGP to hadronic resonance gas at $T_C = 165$ MeV with a relatively long-lived mixed phase. The phase and freeze-out boundaries are shown by the thick lines in Fig. 1. With $T_F = 150$ MeV, the matter lifetime in the center of the system is about 11 fm/c and it decreases towards larger r .

Setup Ia: Hydrodynamics. With the hydrodynamic evolution above, we first assume that the partonic jets lose energy according to Eq. (10) in all phases of QCD matter until $T = T_F$. In Fig. 1, top left panel, we show the paths of zero-rapidity parton jets which are produced at $r = 0$ and 4.5 fm. Choosing a reference time of 1 fm/c, a transport coefficient $\hat{q} = 11.7$ GeV²/fm is determined in the center of the medium by requiring agreement with the measured R_{AA} . From this fit, we get $K = 4.2$,

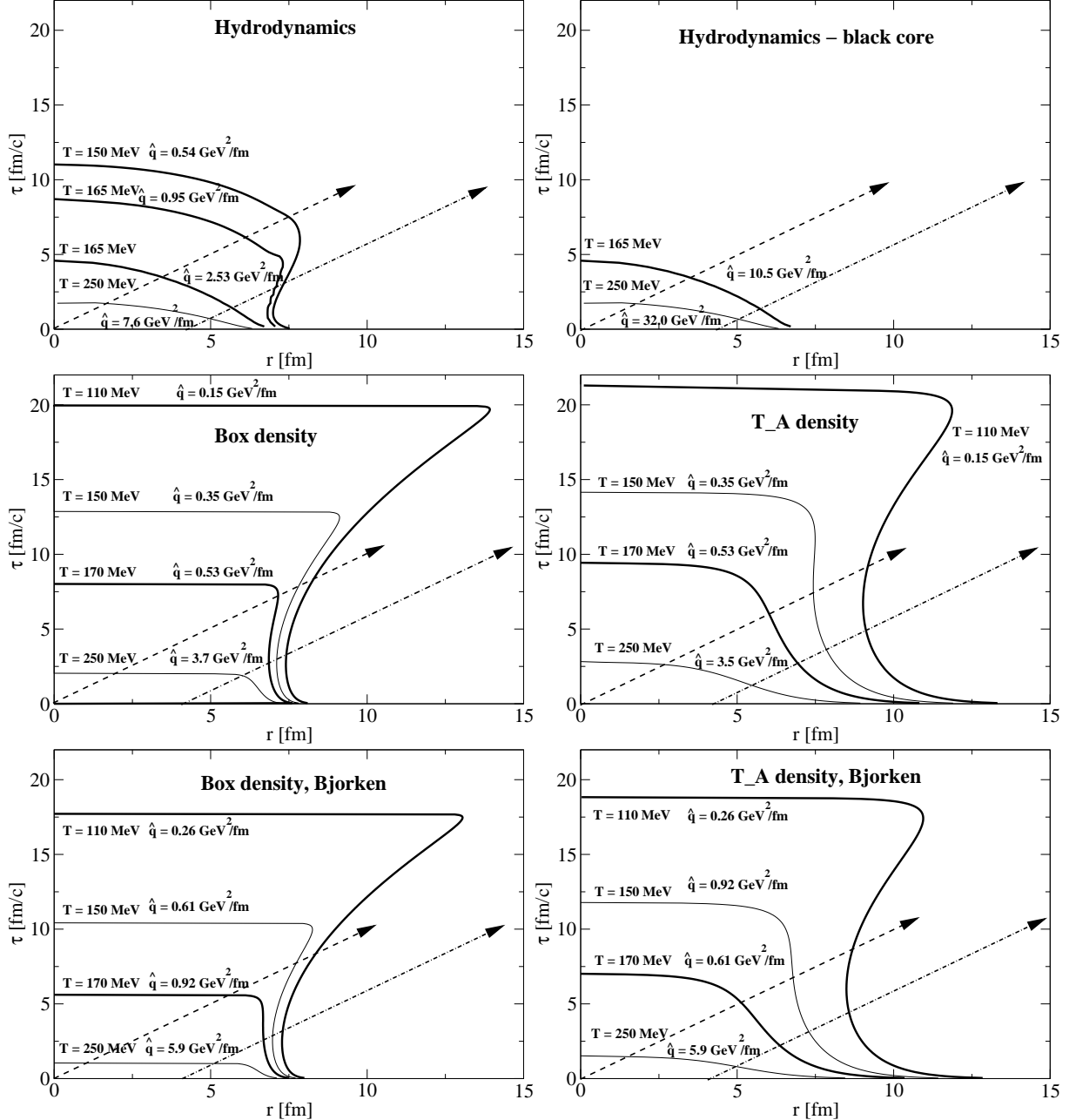


FIG. 1: Equal temperature contour plots for the matter evolution models and energy loss setups described in the text. In the top left panel for the setup Ia, the two lines labelled $T = 165$ MeV show the phase boundary between the QGP and mixed phase, and between the mixed phase and the hadron resonance gas [18]. In the setup Ib, top right panel, only the QGP phase of the hydrodynamic evolution is considered for the partonic energy losses. In the middle and bottom panels for the parametrized evolution model [20] and modifications thereof, the thick lines labelled $T = 170$ MeV represent the isotherm $T = T_C$. The equation of state for these models of Type II contains a cross-over transition, hence no mixed phase appears. The arrows indicate the path of a zero-rapidity hard parton originating from the fireball center $r = 0$ and from $r = 4.5$ fm. The values of \hat{q} along the equal T contours are also indicated.

i.e. there is some deviation from pQCD expectations for the relation Eq. (10).

Setup Ib: Hydrodynamics+Black core. Using the same hydrodynamical model, we make the assumption that energy loss in the medium terminates as soon as $T = T_C$ is reached, i.e. only the QGP

induces energy loss, there is no energy loss for either mixed phase or hadronic gas phase. The top right panel of Fig. 1 illustrates this case. Since the initial distribution of energy density and the distribution of hard vertices both follow $[T_A]^2$, and since the QGP exists only near the center for timescales

$\gg 1 - 2 \text{ fm}/c$, this has the interesting consequence that there is a relatively large halo of vertices surrounding the core from which a hard parton never encounters significant energy loss. In order to compensate for this halo and to agree with the measured R_{AA} the quenching power of the QGP in the core has to be substantial: A fit leads to $K = 17.3$ (i.e. substantial deviations from pQCD expectations) and hence at the reference time of $1 \text{ fm}/c$ the transport coefficient in the medium center is $48.75 \text{ GeV}^2/\text{fm}$. Thus, this scenario is relatively close to geometric suppression in which there is a 'black' region in which hard partons are always absorbed and a 'white' region from which they always escape.

Type II: Parametrized evolution

Setup IIa: Box density. This name denotes the model described in [20] as found in a simultaneous fit to hadron spectra and HBT correlations. It is characterized by a Woods-Saxon density profile with a relatively small surface thickness $d_{ws} \sim 0.5 \text{ fm}$, thus it somewhat resembles a box. This distribution is required by a fit to the HBT correlation radius R_{out} ; as we will argue below in more detail, a sharp transition from medium to vacuum leads to an expanding Cooper-Frye surface and this in turn implies peaked emission during final breakup of the system, i.e. a small emission duration and little difference between R_{out} and R_{side} . There is no microscopic justification to the use of such a steep profile in the initial state however. Since this profile is rather wide, there is no pronounced halo of hard vertices outside the thermalized region.

The model gives a good description of all three HBT correlation radii as well as transverse mass spectra of pions, kaons and protons. It involves (non-Bjorken) accelerated longitudinal dynamics (for details see [20]). This is somewhat beneficial as an initial rapidity interval of ~ 4 units is mapped into a final interval of ~ 7 units, leading to an increased density in the initial state and hence to less deviation from pQCD expectations for K [36]. The equilibration time is $0.6 \text{ fm}/c$. As shown in Fig. 1, middle left panel, for a decoupling temperature $T_F = 110 \text{ MeV}$ the lifetime is about $20.0 \text{ fm}/c$. At the reference time of $1 \text{ fm}/c$, the transport coefficient in the center is $7.11 \text{ GeV}^2/\text{fm}$, corresponding to $K = 2.3$.

Setup IIb: T_A -density Leaving the essential scales of the model [20] as above, we replace the Woods-Saxon density by $T_A(\mathbf{r}_0)$ as could be expected for a soft matter production mechanism. With this modification, the model is still in agreement with hadron spectra and R_{long} but deviates from the measured R_{out} and R_{side} . The transverse profile is still wider than the distribution of production vertices, so no halo is created. With the changed density, the evolution time is $21.5 \text{ fm}/c$, as is demon-

strated by the middle left panel of Fig. 1. At $1 \text{ fm}/c$ evolution time, \hat{q} in the fireball center is $9.9 \text{ GeV}^2/\text{fm}$ using $K = 2.3$.

Setup IIc: Box density+Bjorken. We keep the model as defined above but change longitudinal expansion into a boost-invariant one. This significantly reduces the lifetime to $17.5 \text{ fm}/c$, see Fig. 1 bottom left panel. This is, however, still more than in the hydrodynamical model above which has a much higher decoupling temperature. The resulting evolution is still in fair agreement with R_{side} , but neither R_{out} nor R_{long} can be described. At the reference time, this leads to $\hat{q} = 6.85 \text{ GeV}^2/\text{fm}$ in the fireball center using $K = 4.0$.

Setup IId: T_A -density+Bjorken. As above, but we change the transverse density profile into the T_A density. The resulting fireball lifetime is $18.5 \text{ fm}/c$, see Fig. 1 bottom right, and at the reference time we find $\hat{q} = 9.4 \text{ GeV}^2/\text{fm}$ in the fireball center using $K = 4.0$.

As discussed in [36], the deviation of K from 1 is predominantly influenced by assumptions about the longitudinal flow and to 2nd order also determined by the magnitude of transverse flow.

We note at this point that a measurement of the longitudinal expansion dynamics can be done e.g. using thermal photons [43]. Fixing the precise value of K would clearly increase the value of dihadron correlations as a tool for medium tomography.

While the models presented here are far from being an exhaustive search through the parameter space of reasonable bulk matter evolution models, we believe they represent a fair sample by including two different types of longitudinal dynamics, three different assumption about the transverse density profile and three variations in the decoupling parameters.

III. SINGLE HADRON OBSERVABLES

Let us start with a discussion of R_{AA} and the modification of single hadron spectra in the model. The models describe R_{AA} rather well using a single adjustable parameter K . The quality of the description is shown for the hydrodynamical model in Fig. 2, it is comparable for the other models (not shown).

A. High opacity saturation

In [39, 44] it was argued, albeit based on simulations in static scenarios, that R_{AA} for $\hat{q} > 5 \text{ GeV}^2/\text{fm}$ gradually loses the sensitivity to energy densities in the medium core, hence the observed amount of high p_T hadrons has a high probability to come from the surface. As is evident from the previous section, \hat{q} is for some time in all of the models of that order (however, due to the expansion and subsequent dilution drops at later times).

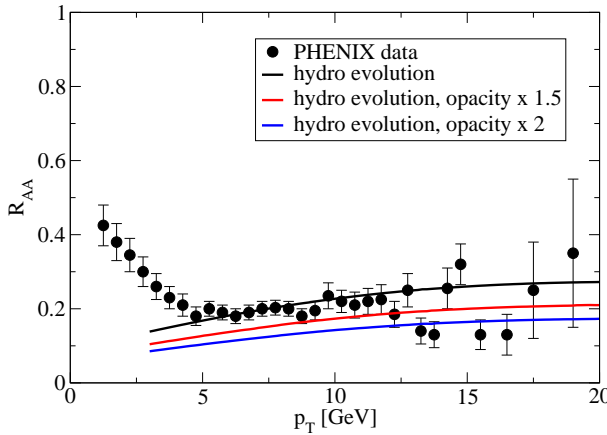


FIG. 2: Model calculation of the nuclear suppression factor R_{AA} as compared to PHENIX data [45] for the best fit within the hydro model, setup Ia, (see text) and with additional increase of the medium opacity by 50 and 100%. In the other setups, the shape and magnitude of R_{AA} are practically identical to this figure.

In our dynamical framework, we can test this by increasing the value of K beyond the best fit to the data. This directly scales the medium opacity. In Fig. 2 we show the best fit to R_{AA} with the hydrodynamical models with parameters as given in section II D. This gives a fair description of the measured pionic R_{AA} beyond $p_T = 5$ GeV. Increasing the opacity by 50 and 100% apparently leads to some kind of saturation, but the limiting curve for further increases of opacity is clearly below the data in the region between 5 and 15 GeV transverse momentum. Thus, the conclusion is that if the full dynamics is taken into account, saturation of R_{AA} with respect to increasing \hat{q} and dominance of surface emission is not yet reached.

B. The geometry underlying R_{AA}

We can gain further insight into the question of surface vs. volume dominated emission by studying the origin of trigger hadrons from the MC simulations. These contain the same information as R_{AA} , albeit in more differential form at a given scale (i.e. the trigger momentum). This is shown in Fig. 3.

As evident from the figure, while there is some degree of surface bias and little emission is found from the fireball core, the spatial region probed by a single hadron distribution extends deep into the medium. The only scenario where this is not quite the case is the 'black core' hydrodynamics. Here, a clear trend to surface emission is visible, although still the core is not completely black.

It is evident that the degree of surface bias is model dependent. We find consistently that in scenarios in which the initial distribution of matter is rather wide (and correspondingly the local \hat{q} can be smaller to achieve the

same R_{AA}) the degree of surface bias is reduced. There is also some sensitivity to the underlying density profile visible in the comparison of the box and T_A density scenarios. This gives some confidence that once the away side parton is considered, its sensitivity to $\langle P(\Delta E) \rangle_{Tr}$ will be able to distinguish two scenarios which are characterized by the same $\langle P(\Delta E) \rangle_{T_{AB}}$ but have different distributions of matter.

C. The role of transverse flow

Let us at this point briefly remark on the role of transverse flow. In [17] it was pointed out that this is a crucial effect for long pathlength and increases the transparency of the medium. While the transverse geometry does not change significantly for timescales of 2-3 fm after equilibration since transverse flow takes some time to develop, the change of transverse geometry by transverse flow clearly is an issue for longer timescales (which, according to Fig. 3 are frequently probed even for single hadron observables when the vertex lies close to the fireball center).

It is sometimes argued that the effect of transverse flow cancels for radiative energy loss with a quadratic dependence on pathlength. This argument goes as follows: Suppose we have a homogeneous medium with expands with the velocity v_T in radial direction. The medium density (and hence the transport coefficient) drops like $1/(v_T \tau)^2$ due to the transverse expansion. However, the freeze-out surface also moves outward with v_T , and hence there is an additional pathlength $\sim v_T \tau$ the particle has to go through the medium. For quadratic pathlength dependence of energy loss, this implies additional energy loss $\sim (v_T \tau)^2$ which would just cancel the effect of the dropping transport coefficient in Eq. (8).

What is missing in the argument is that an actual medium is not homogeneous, and therefore the Cooper-Frye surface does in general not expand with the flow lines. Only in the case of a homogeneous box density profile is this the case, for any realistic density profile the Cooper-Frye expands much more weakly or even shrinks in time. This can clearly be seen e.g. in Fig. 2 of Ref. [18]. However, especially in scenarios where the Cooper-Frye surface shrinks with time, transverse flow has an enormous impact — not only is the density dropping with $(v_T \tau)^2$ but there is also a systematic shortening of the in-medium paths. Thus, transverse flow can, contrary to the naive expectation, have a significant impact on the medium transparency.

D. Average quenching properties

In Fig. 4 we show the average energy loss per unit time (unit pathlength) as a function of time for a quark starting from the center $r = 0$ of the fireball and from the

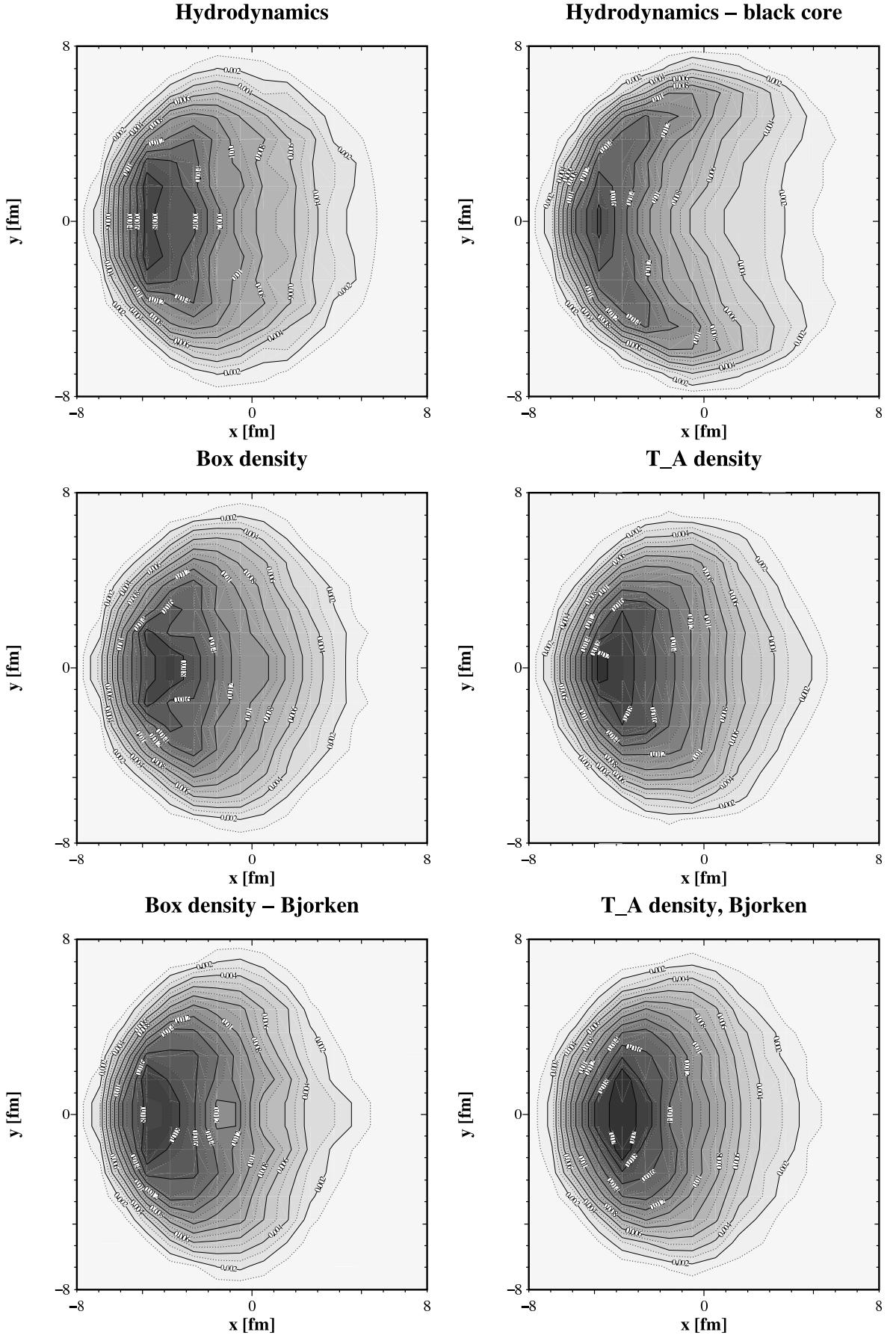


FIG. 3: Probability density of finding a parton production vertex at (x, y) given a triggered event with $8 \text{ GeV} < p_T < 15 \text{ GeV}$ for different spacetime evolution scenarios (see text). In all cases the near side (triggered) hadron propagates to the $-x$ direction, hence the $y - (-y)$ symmetrization. Contours are at linear intervals.

typical emission region (the maximum seen in Fig. 3, $r \approx 4.5$ fm). We obtain this quantity via

$$\langle \Delta E \rangle = \int_0^\infty P(\Delta E)_\tau \Delta E d\Delta E \quad (21)$$

with $P(\Delta E)_\tau$ obtained with the help of the line integrals Eq. (8) and Eq. (9) with the upper integration limit changed into τ . Interestingly enough, the total average energy loss in all scenarios is between 20 and 23.5 GeV for a quark (between 34 and 37 GeV for a gluon), although evolution of the loss per unit pathlength is quite different in the different models. One may speculate that this is caused by the fact that all scenarios describe R_{AA} by construction. Since the measured value of R_{AA} can be understood by the observation that about 80% of all partons are not observed in the perturbative region and since most partons originate from the region around the medium core, the similarity of the average energy lost presumably also ensures that the probability distribution of energy loss for the typical parton from the central region is comparable and hence a similar fraction of absorbed partons from this dominant central region observed. However, the origin of the observed minority of partons is quite different in all cases.

Qualitatively, all curves exhibit the same shape. First, there is a strong rise: As pathlength increases, it allows for decoherence of softer and softer quanta (parametrically the decoherence length of a radiated quantum with momentum q_T transverse to the hard parton and energy ω goes like $\tau_{dec} \sim \omega/k_T^2$; however soft quanta are more likely to be radiated) [23]. In a static, homogeneous medium this feature leads to the quadratic pathlength dependence of radiative energy loss. In a dynamic evolution, there is eventually a turnover as the density of the medium is decreased, either because volume expansion dilutes the medium over time or because the parton reaches the thinner outer layers of the transverse density profile. This turnover point is model dependent: for the hard partons produced in the fireball center (left panel), the average energy loss per time peaks at 1-3 fm for the hydrodynamic scenarios Ia,b, and at 2-4 fm for the setups IIa-d. This implies that if a parton can escape the medium during the first 1-2 fm/c evolution time it will never undergo substantial energy loss (this is not quite true in the 'black core' scenario though). Thus, the halo region where partons are not strongly medium modified may be expected to reach into the medium at least 1-2 fm beyond the position of the Cooper-Frye surface; dependent on the density profile at the outer edge of the medium even further.

The later flattening of the curve, most pronounced in the hydrodynamical evolution after about 4 fm/c is related to the slowdown of the expansion rate in the mixed phase when the pressure of the medium vanishes and accelerated transverse expansion turns to constant transverse expansion. This feature is less pronounced in the parametrized evolution scenarios as these employ a

crossover transition where a soft point in the EOS is reached but the transverse acceleration never drops to zero.

In the 'black core' scenario, the average energy loss of partons released from the center gets as high as 18 GeV/fm and even in the least dramatic box density case it reaches up to 4 GeV/fm. Thus, it is safe to conclude that the medium is on average extremely black — propagation of partons from the medium core to the surface would take of the order of 25 GeV parton energy, thus the typical parton energy before energy loss and fragmentation would have to be ~ 40 GeV to form a 8 GeV hadron, a scale far above typical parton energies available in significant numbers. We therefore conclude that fluctuations around the average energy loss must be large. In a situation in which partons are absorbed by the medium on average, fluctuations will open up the possibility of the parton being able to penetrate the medium and hence increases the transparency somewhat. Let us explore this by studying a probabilistic representation of the quenching process in the model.

E. Averaged energy loss probabilities

We show the geometry-averaged energy loss probabilities for quarks $\langle P(\Delta E) \rangle_{T_{AA}}$ (see Eq. (15)) for the different scenarios in Fig. 5. This quantity reinforces our conclusion from the average energy loss: Typically quenching is substantial, but there are strong fluctuations. The probability distributions exhibit long tails extending out above 100 GeV energy loss, but there is also a large escape probability of 0.26 for the hydrodynamics case, 0.3 for the black core case and 0.24 for all other scenarios. Note that all parametrized evolutions lead to virtually the same averaged energy loss probability — they would be indistinguishable even by a γ -hadron correlation measurement as outlined in [8].

Taking gluons into account, there is little actual energy loss observed in the model: About 15-20% of the partons escape without energy loss (either because they are created outside the medium or due to fluctuations in the energy loss probability), only about 5-8% of partons contribute to the hard hadron spectrum after undergoing some energy loss and 75-80% of partons are absorbed in the medium and thermalize. Thus, the information about the medium is predominantly carried in the ratio of absorption to transmission, not in the average energy loss of observed hadrons.

This has been observed in [17, 39] already and seems to be characteristic for the BDMPS energy loss in the formalism of [23] in the RHIC energy range as long as a realistic distribution of pathlengths is taken into account. Thus, if BDMPS energy loss is realized in nature, one has to go even beyond γ -hadron correlations (which reflect the $[T_A(r)]^2$ profile of the hard vertices) to gain sensitivity to details of the medium density distribution.

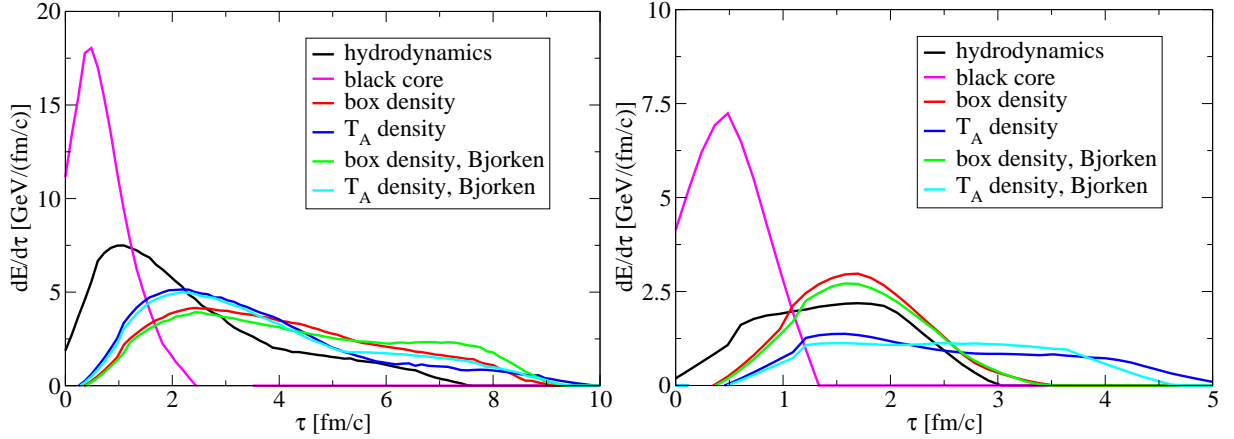


FIG. 4: Left panel: Average energy loss per time for a hard quark released in the fireball center $r = 0$ propagating towards the surface for the different setups studied. Right panel: Same quantity but for a quark propagating outwards from the maximum of emissivity seen in Fig. 3, i.e. about 4.5 fm from the center. Notice the difference in the horizontal scales.

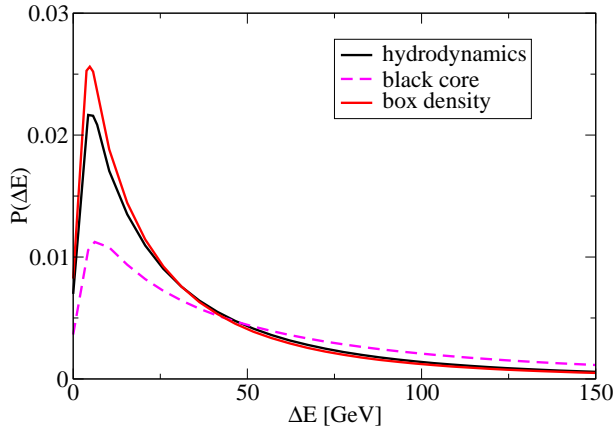


FIG. 5: Geometry-averaged energy loss probability $\langle P(\Delta E) \rangle_{TAA}$ of quarks for different spacetime evolution scenarios (T_A -density, box density Bjorken and T_A density Bjorken are not shown, they are indistinguishable from the box density scenario).

In the following, we explore the possibility of doing this in hard back-to-back correlations of hadrons.

IV. DIHADRON OBSERVABLES

Let us at this point remark that back-to-back dihadrons are a rare event and do not reveal the typical situation of a parton pair emerging from a hard vertex but rather a highly unlikely coincidence. About 4 out of 5 partons potentially leading to a hard trigger above 8 GeV are absorbed by the medium, and the yield per trigger on the away side is on the order of 2% [15, 16], thus there is massive additional suppression. However, much of this is due to the low probability of a hard away side parton to fragment into a hard hadron. Taking this effect into consideration by comparing with the d-Au data, the ad-

ditional suppression of the away side is about of the same order as the near side suppression — roughly 4 in 5 of partons back to back with a valid trigger are quenched. This is an interesting observation in itself, as it clearly demonstrates that the systematic difference in path-length between near and away side is important. This essentially rules out a purely geometric interpretation of jet quenching where partons born in a 'black' region are always absorbed and partons born in a 'white' region always survive — in such a scenario there would be no additional absorption of away side partons and the yield per trigger (modulo fragmentation) would be of order one. But it also places strong constraints on the time cutoff of quenching — if the medium becomes transparent due to the volume expansion too soon, there is no time for the away side partons to pick up additional energy loss due to their longer in-medium path. Unfortunately, in order to make these statements quantitative, a microscopic description of jet energy loss including the full geometry (vertex distribution in Fig. 3) is required. Since we have limited ourselves in the present investigation to BDMPS radiative energy loss, we will not explore this interesting possibility further here but rather leave this to a subsequent publication.

A. The geometry of dihadron correlations

We show the probability density of vertices in the (x, y) plane leading to a near side trigger hadron above 8 GeV and an associate away side hadron with $4 \text{ GeV} < p_T < 6 \text{ GeV}$ in Fig. 6. It is immediately obvious that the distribution is very different from the distribution of vertices for single hadron observation shown in Fig. 3. First, the dihadron distributions are much wider in $\pm y$ direction, indicating the importance of the periphery where both near and away side parton have a short in-medium path (or the halo where the production vertex lies outside the

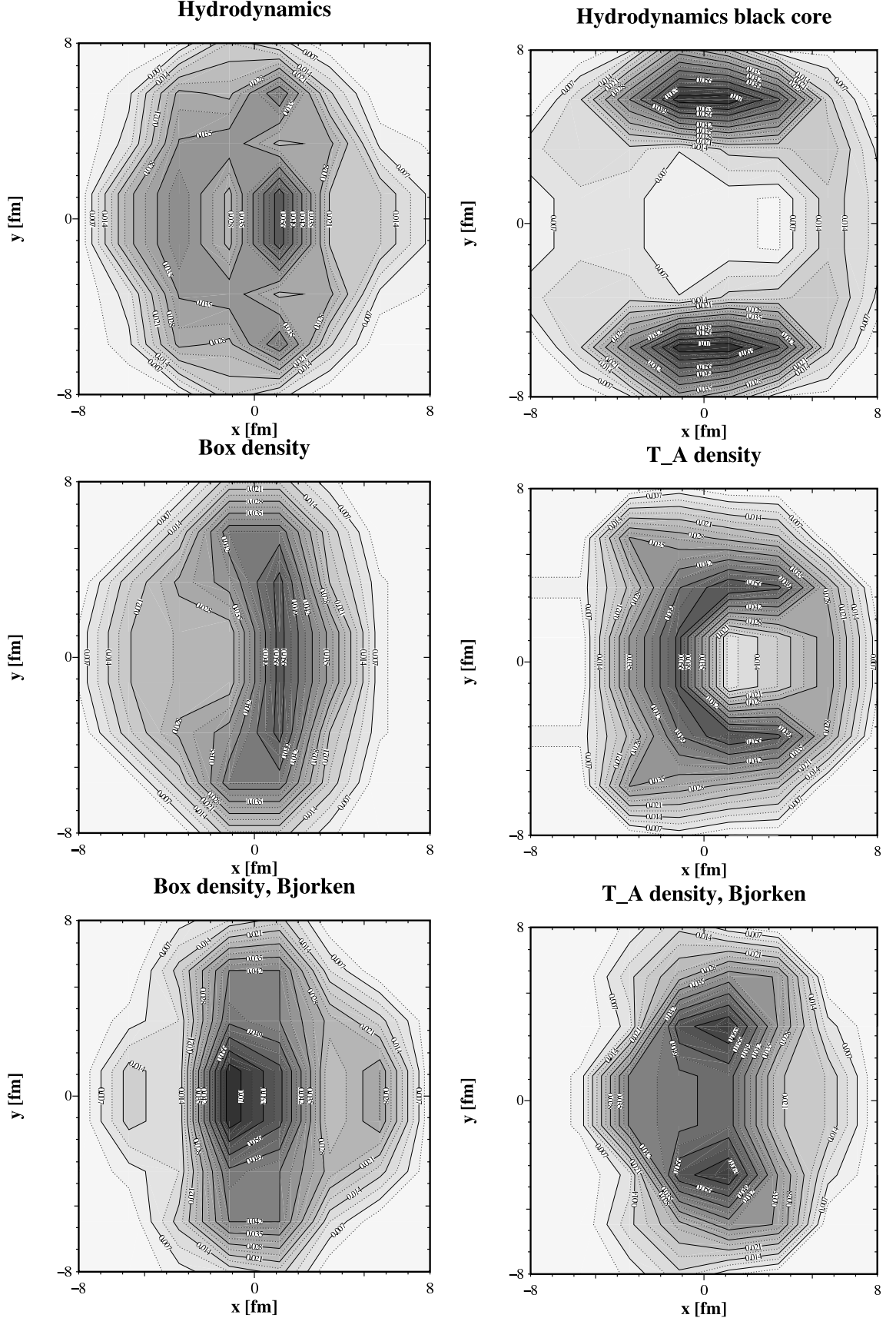


FIG. 6: Probability density for finding a vertex at (x, y) leading to a triggered event with $8 \text{ GeV} < p_T < 15 \text{ GeV}$ and in addition an away side hadron with $4 \text{ GeV} < p_T < 6 \text{ GeV}$ for different spacetime evolution scenarios (see text). In all cases the near side hadron propagates to the $-x$ direction.

medium). This is most clearly seen for the black core scenario where there is almost complete repulsion of events from the dense core to the periphery.

The second observation is that while the single hadron vertex distributions are typically centered around $x \sim -4 \dots -5$ fm, the dihadron distributions roughly center around $x \sim 0$ where both near and away side have similar pathlengths. Clearly there is also pronounced sensitivity to the medium density — in both T_A density scenarios the distribution is repelled from the center of the fireball by the peak in medium density — no such trend is seen for the box densities (where no pronounced peak in the fireball center is present). Thus, just based on the observed geometry one would conclude that there is significantly more sensitivity to medium properties in dihadron correlations than in single hadron suppression.

B. Comparison with STAR data

We show the results of the model calculation for near and away side yields per trigger for a trigger of $8 \text{ GeV} < p_T < 15 \text{ GeV}$ as a function of associate hadron momentum bin in comparison with the data [15, 16] for central collisions in Fig. 7.

Within errors, the near side yield per trigger is described by all the models well. There is no significant disagreement among the models. This is not very surprising — as we have seen above and remarked in [17], about 80% of all near side partons emerge from the medium without having experienced energy loss. Thus, it is not expected that energy loss is able to modify the next-to-leading fragmentation of the trigger parton significantly.

The model calculations appear significantly more different if we consider the away side yield. Here, results for the 4-6 GeV momentum bin differ by almost a factor two. However, none of the model calculations describes the data in this bin. This is in fact not at all surprising as below 5 GeV the inclusive single hadron transverse momentum spectra are not dominated by pQCD fragmentation and energy losses but, rather, by hydrodynamics possibly supplemented with recombination [46] type phenomena, see Fig. 9 of Ref. [18]. For this reason, the ratio R_{AA} at $p_T < 5 \text{ GeV}$ cannot be expected to be described by pQCD fragmentation and energy losses, either. In Ref. [18], it was also argued that the hydrodynamic and pQCD components of the single hadron spectra are to a good degree independent. Thus, while the near side trigger hadron at 8 GeV and above clearly originates from a pQCD vertex, the associate hadron on the away side observed at 4-5 GeV originates most likely from the bulk (described by hydro and recombination) rather than from the same pQCD vertex as the triggered hadron. In this light, it would be a mere coincidence if a good agreement of the low-energy bin on the away side were obtained between the data and our calculation. We conclude that our model cannot offer a reliable prediction of away side hadronic yields in this bin.

This is clearly unfortunate, as the model results are considerably closer to the experimental result in the 6+ momentum bin on the away side and hence our ability to discriminate between different models is reduced. Since at this large transverse momenta the pQCD fragmentation + energy losses dominate the single hadron spectrum (again see Fig. 9 of Ref. [18]), we expect that the model is able to give a valid description of the relevant physics in this bin: Not only is R_{AA} well described by the data, but also the contribution of recombination processes to the yield is expected to be small [46]. Thus, as it stands, only the black core scenario can be ruled out by the data, the box density with Bjorken expansion seems strongly disfavoured but still marginally acceptable. In a sense this is certainly reassuring, as this identifies the scenario least likely to be realized in heavy-ion collisions — the black core scenario exhibits strong deviations from pQCD expectations for the energy loss and there is no a priori reason that the mixed phase or the hadron gas should not contribute to energy loss.

Nevertheless, while there are indications that the other scenarios show sizable differences in the momentum spectrum of away side hadrons, the present data is not sufficient to make a distinction. There are in principle two ways to overcome this problem. At the price of introducing additional model dependence, one might include recombination processes into the simulation. In this way, comparison to the 4-6 GeV momentum bin would be possible. Alternatively, one can address the question if more leverage in p_T would improve the question and hence if improved experimental conditions will allow tomography. We have chosen to follow the latter path. Towards this end, we study in the following a situation where the trigger momentum is increased to $15 \text{ GeV} < p_T < 20 \text{ GeV}$ and consequently more momentum bins in the pQCD region become accessible.

C. Partonic and hadronic momentum spectra for $p_T > 15 \text{ GeV}$ trigger conditions

We present the distribution of away side parton momenta given a hard triggered hadron on the near side in Fig. 8 before (left panel) and after (right panel) energy loss due to the medium. The spread of the distribution before energy loss is a measure for the amount of energy loss (as compared to transmission or absorption) induced by the scenarios; or equivalently, the similarity of the curves restates the fact that the geometry-averaged distributions $\langle P(\Delta E) \rangle_{T_{AA}}$ are rather similar.

Considering the distribution after energy loss (and disregarding again the dominant absorption contribution), there is a sizable shift of the spectral distribution towards lower momenta, but this shift is different for the different models. Clearly, the black core model is most extreme, but differences of the order of 20-30% are also seen in the other models.

The distribution after fragmentation into hadrons in bins

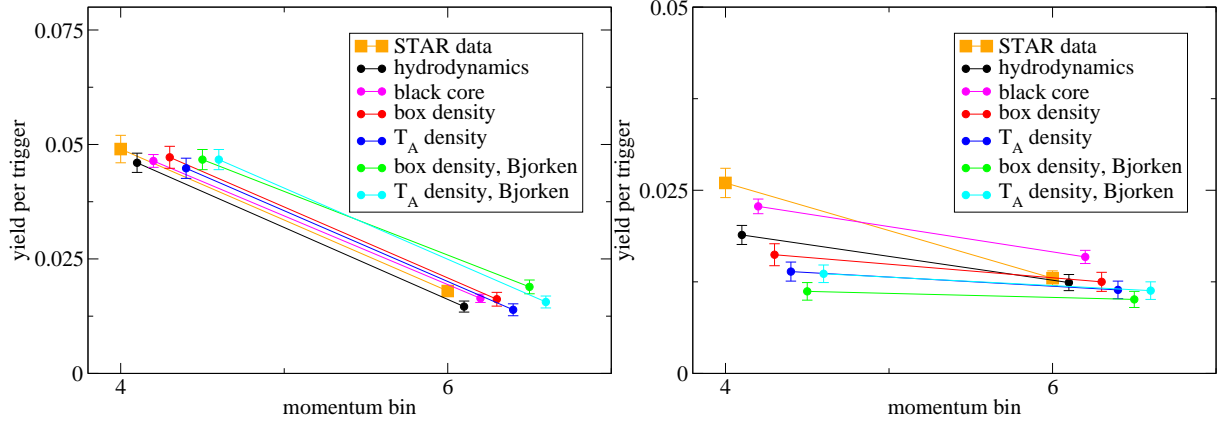


FIG. 7: Yield per trigger on the near side (left panel) and away side (right panel) of hadrons in the 4-6 GeV and 6+ GeV momentum bin associated with a trigger in the range $8 \text{ GeV} < p_T < 15 \text{ GeV}$ for the different models of spacetime evolution as compared with the STAR data [15, 16]. The individual data points have been spread artificially along the x axis for clarity of presentation.

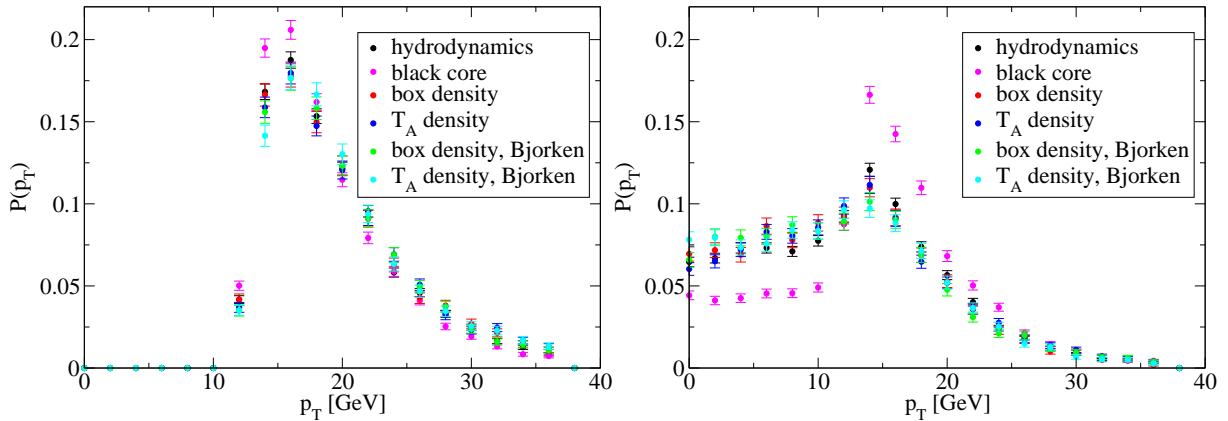


FIG. 8: Probability distribution $P(p_T)$ to find momentum p_T for the away side parton given a triggered hadron in the range $15 \text{ GeV} < p_T < 20 \text{ GeV}$ before (left panel) and after (right panel) energy loss due to passage through the medium for different spacetime evolutions. Here, we only consider away side partons not absorbed by the medium.

of 2 GeV width in the perturbative region is shown in Fig. 9 for the near side (left panel) and away side (right panel). It is again apparent that within errors all models agree in the expected near side yield. The momentum spectrum of the away side exhibits considerably more structure. Several of the scenarios can now be clearly told apart in bins in the perturbative region. For example the T_A and the box density which have virtually identical $\langle P(\Delta E) \rangle_{T_{AA}}$ (cf. Fig. 5) show almost a factor two difference in the 10-12 GeV momentum bin; T_A and T_A Bjorken can be told apart in the 6-8 GeV momentum bin (provided enough experimental precision is achieved).

It is evident from the analysis that having a larger lever-arm in momentum is clearly beneficial — as apparent from the figure, the momentum distribution of away side hadrons after energy loss with $\langle P(\Delta E) \rangle_{\text{trigger}}$ is characteristic of the scenario, and although the differences induced by the different geometry and expansion pattern are not factors of 10, they may reach as much as 50%.

D. Changes in geometry with trigger and associate energy

In Fig. 10 we investigate to what degree the region in the transverse plane probed by the dihadron correlation is changed with increased trigger momentum and/or associate cut. We do this at the example of the hydrodynamical evolution.

In the left panel, we show the distribution of vertices leading to an away side hadron between 4 and 6 GeV, but for a trigger hadron above 15 GeV. Comparing Figs. 10 and 6, there is (given the limited statistics) no significant difference between the figures.

However, going to higher associate hadron momentum between 8 and 10 GeV, we find that the distribution is somewhat more pushed out of the fireball center. Apparently, in this case even small energy loss is disfavoured. But all in all, the influence of the spacetime distribution of matter on the probability distribution of vertices is

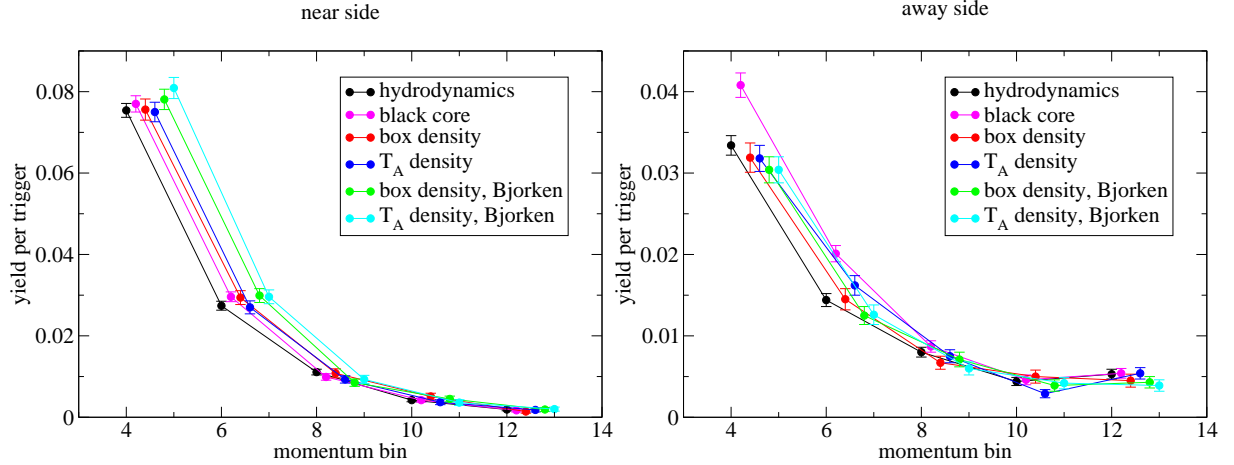


FIG. 9: Yield per trigger on the near side (left panel) and away side (right panel) of hadrons in the 4-6 GeV, 6-8 GeV, 8-10 GeV, 10-12 GeV and 12+ GeV momentum bin associated with a trigger in the range $15 \text{ GeV} < p_T < 20 \text{ GeV}$ for the different models of spacetime evolution. The individual data points have been spread artificially along the x axis for clarity of presentation. Note that the last bin extends from 12 GeV up to the p_T of the trigger hadron and is thus considerably wider than the previous bin, explaining the upward turn of some spectra.

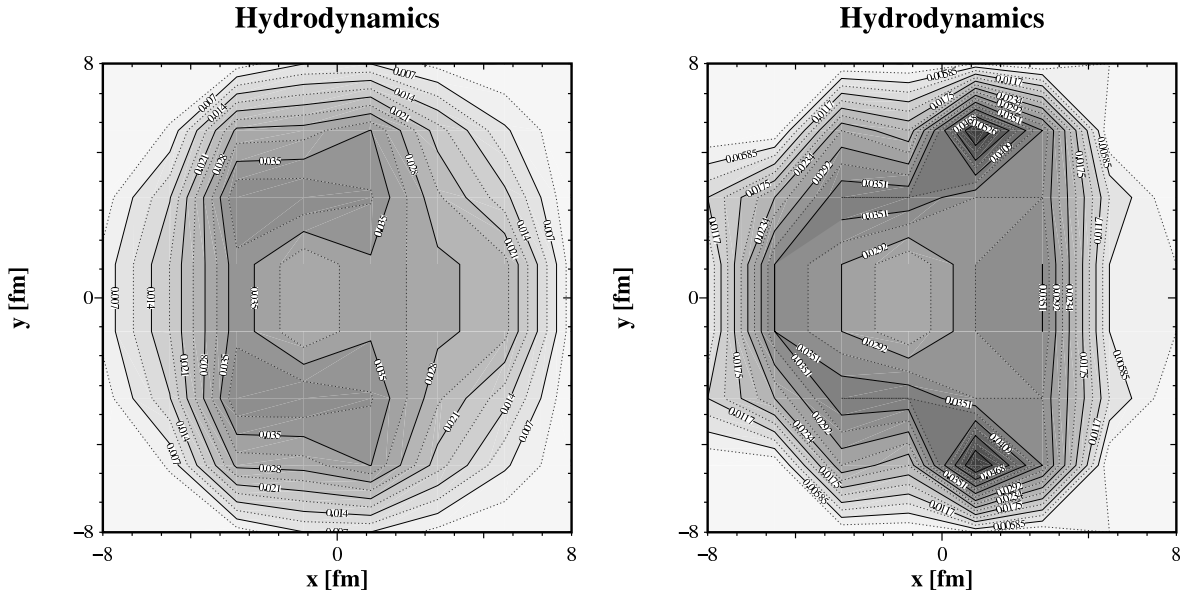


FIG. 10: Probability density for finding a vertex at (x, y) leading to a triggered event with $15 \text{ GeV} < P_T < 20 \text{ GeV}$ and in addition an away side hadron with $4 \text{ GeV} < P_T < 6 \text{ GeV}$ (left panel) and $8 \text{ GeV} < P_T < 10 \text{ GeV}$ (right panel) for the hydrodynamical evolution model. In all cases the near side hadron propagates to the $-x$ direction.

greater than the influence of trigger and associate momentum scaling.

E. High opacity saturation?

Since hard dihadron correlations select a special class of events with an underlying vertex distribution very different to the distribution underlying any single hadron

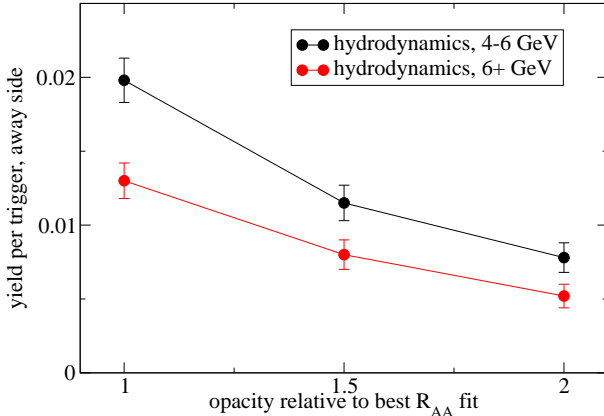


FIG. 11: Model calculation of the away side yield per trigger for an $8 < p_T < 15$ GeV hadron trigger in two different momentum bins as compared to STAR data [15, 16] for the hydro model, setup Ia, (see text) and with additional increase of the medium opacity by 50 and 100%.

observable, it is useful to investigate the question if any saturation of the yield with the quenching power of the medium is reached. Note that there is no a priori reason to expect the density at which single and dihadron observables saturate to be the same, as dihadron observables probe the quenching of rare fluctuations in the energy loss probability distribution.

As in the case of R_{AA} , we can test this by increasing the value of K beyond the value obtained from a fit to R_{AA} . We show the resulting reduction in the away side yield per trigger in Fig. 11 calculated within the hydro model setup Ia. There is some flattening of the curves observed but no saturation of the yield within the opacity given by the model. This observation is consistent with the information from Fig. 6 where it is clearly seen that apart from the black core scenario hard dihadrons originate from the medium center and are not yet pushed out to the periphery by unpenetrable central densities of the medium. The fact that saturation of R_{AA} appears to be reached earlier than saturation of the away side yield in dihadron correlations, in particular in the 6+ momentum bin, is also consistent with the observation that single hadron observables show generally more surface bias (see Fig. 3).

V. DISCUSSION

We have studied the possibility of doing jet tomography, i.e. discriminating structures of the density distribution

and the expansion pattern of the medium created in ultrarelativistic heavy-ion collisions using back-to-back correlations of hard hadrons.

We found that due to the different geometry entering the averaged energy loss probability distributions $\langle P(\Delta E) \rangle_{T_{AB}}$ and $\langle P(\Delta E) \rangle_{Tr}$ there is non-trivial information in the dihadron yield per trigger beyond what is constrained by R_{AA} . We have explicitly shown that even the current data are able to rule out a somewhat more extreme scenario of jet quenching and that a greater lever-arm in away side hadron momentum offers the possibility to discriminate scenarios which lead to the same $\langle P(\Delta E) \rangle_{T_{AB}}$ and are hence even in principle indistinguishable by either R_{AA} or γ -hadron correlation measurements.

The requirement of having a large number of momentum bins to get better discrimination however makes this method in all likelihood more suitable for the LHC where hadrons up to 100 GeV momentum are expected to be observed regularly and thus a large number of momentum bins could be measured with great precision far in the spectral region where pQCD and vacuum fragmentation is applicable.

Given the large possible parameter space of medium evolution models, it is unlikely that any form of jet tomography alone will yield a complete characterization of the medium density. It seems rather that a multi-pronged approach, i.e. simultaneously measuring γ -hadron correlations (and hence $\langle P(\Delta E) \rangle_{T_{AB}}$ for quarks), back-to-back correlations (i.e. $\langle P(\Delta E) \rangle_{Tr}$), thermal photons (sensitive to the longitudinal expansion [43]) and a reaction plane analysis of R_{AA} [47] introducing a handle on the systematic variation of the in-medium pathlength distribution will be a suitable tool to extract tomographic information using hard probes.

Acknowledgments

We would like to thank Jan Rak, Peter Jacobs, Vesa Ruuskanen, Jörg Ruppert and Harri Niemi for valuable comments and discussions. This work was financially supported by the Academy of Finland, Project 206024. The numerical Monte Carlo simulations were carried out at the NERSC scientific computing center at Lawrence Berkeley National Laboratory.

[1] K. Adcox *et al.* [PHENIX Collaboration], Nucl. Phys. A **757** (2005) 184; J. Adams *et al.* [STAR Collaboration], Nucl. Phys. A **757** (2005) 102; B. B. Back *et al.* [PHOBOS Collaboration], Nucl. Phys. A **757** (2005) 28; I. Arsene *et al.* [BRAHMS Collaboration], Nucl. Phys. A **757** (2005) 1.

- [2] M. Gyulassy and X. N. Wang, Nucl. Phys. B **420**, (1994) 583.
- [3] R. Baier, Y. L. Dokshitzer, A. H. Mueller, S. Peigne and D. Schiff, Nucl. Phys. B **484**, (1997) 265.
- [4] B. G. Zakharov, JETP Lett. **65**, (1997) 615.
- [5] U. A. Wiedemann, Nucl. Phys. B **588**, (2000) 303.
- [6] M. Gyulassy, P. Levai and I. Vitev, Nucl. Phys. B **594**, (2001) 371.
- [7] X. N. Wang and X. F. Guo, Nucl. Phys. A **696**, (2001) 788.
- [8] T. Renk, hep-ph/0607166.
- [9] S. S. Adler *et al.* [PHENIX collaboration], nucl-ex/0507004.
- [10] T. Renk and J. Ruppert, Phys. Rev. C **73**, (2006) 011901.
- [11] J. Casalderrey-Solana, E. V. Shuryak and D. Teaney, hep-ph/0411315.
- [12] H. Stoecker, Nucl. Phys. A **750** (2005) 121.
- [13] J. Ruppert and B. Muller, Phys. Lett. B **618** (2005) 123.
- [14] T. Renk and J. Ruppert, in preparation.
- [15] D. Magestro [STAR Collaboration], nucl-ex/0510002; talk Quark Matter 2005.
- [16] J. Adams *et al.* [STAR Collaboration], nucl-ex/0604018.
- [17] T. Renk, Phys. Rev. C **74** (2006) 024903..
- [18] K. J. Eskola, H. Honkanen, H. Niemi, P. V. Ruuskanen and S. S. Rasanen, Phys. Rev. C **72** (2005) 044904.
- [19] K. J. Eskola, K. Kajantie, P. V. Ruuskanen and K. Tuominen, Nucl. Phys. B **570** (2000) 379.
- [20] T. Renk, Phys. Rev. C **70** (2004) 021903.
- [21] I. G. Bearden *et al.* [BRAHMS Collaboration], Phys. Rev. Lett. **88** (2002) 202301.
- [22] S. S. Adler *et al.* [PHENIX Collaboration], Phys. Rev. Lett. **93** (2004) 152302.
- [23] C. A. Salgado and U. A. Wiedemann, Phys. Rev. D **68**, (2003) 014008.
- [24] K. J. Eskola and H. Honkanen, Nucl. Phys. A **713** (2003) 167.
- [25] J. Pumplin, D. R. Stump, J. Huston, H. L. Lai, P. Nadolsky and W. K. Tung, JHEP **0207**, (2002) 012.
- [26] D. Stump, J. Huston, J. Pumplin, W. K. Tung, H. L. Lai, S. Kuhlmann and J. F. Owens, JHEP **0310**, (2003) 046.
- [27] M. Hirai, S. Kumano and T. H. Nagai, Phys. Rev. C **70**, (2004) 044905.
- [28] K. J. Eskola, V. J. Kolhinen and C. A. Salgado, Eur. Phys. J. C **9** (1999) 61.
- [29] I. Sarcevic, S. D. Ellis and P. Carruthers, Phys. Rev. D **40**, (1989) 1446.
- [30] B. A. Kniehl, G. Kramer and B. Potter, Nucl. Phys. B **582**, (2000) 514.
- [31] R. Baier, Nucl. Phys. A **715**, (2003) 209.
- [32] A. Peshier, hep-ph/0607275.
- [33] S. Wicks, W. Horowitz, M. Djordjevic and M. Gyulassy, nucl-th/0512076.
- [34] H. Liu, K. Rajagopal and U. A. Wiedemann, hep-ph/0605178.
- [35] C. A. Salgado and U. A. Wiedemann, Phys. Rev. Lett. **89**, (2002) 092303.
- [36] T. Renk and J. Ruppert, Phys. Rev. C **72** (2005) 044901.
- [37] N. Armesto, C. A. Salgado and U. A. Wiedemann, Phys. Rev. C **72**, (2005) 06491.
- [38] U. A. Wiedemann, private communication.
- [39] A. Dainese, C. Loizides and G. Paic, Eur. Phys. J. C **38**, (2005) 461.
- [40] K. J. Eskola, H. Niemi, P. V. Ruuskanen and S. S. Rasanen, Phys. Lett. B **566** (2003) 187.
- [41] K. J. Eskola and K. Tuominen, Phys. Rev. D **63** (2001) 114006; K. J. Eskola and K. Tuominen, Phys. Lett. B **489** (2000) 329.
- [42] S. S. Adler *et al.* [PHENIX Collaboration], Phys. Rev. C **69** (2004) 034909.
- [43] T. Renk, Phys. Rev. C **71** (2005) 064905.
- [44] K. J. Eskola, H. Honkanen, C. A. Salgado and U. A. Wiedemann, Nucl. Phys. A **747** (2005) 511.
- [45] M. Shimomura [PHENIX Collaboration], nucl-ex/0510023.
- [46] R. J. Fries, B. Muller, C. Nonaka and S. A. Bass, Phys. Rev. C **68** (2003) 044902.
- [47] A. Majumder, nucl-th/0608043.